Hoop Stress Modification, Stress Hysteresis and Degradation of a REBCO Coil Due to the Screening Current Under External Magnetic Field Cycling

Shunji Takahashi, Yu Suetomi, Tomoaki Takao, Yoshinori Yanagisawa, Hideaki Maeda, Yasuaki Takeda, and Jun-ichi Shimoyama

***Abstract*—Degradation of a REBCO coil under external magnetic fields is one of the major technical problems in the field of HTS magnet technology. A possible cause of such degradation is an inhomogeneous hoop stress distribution, or hoop stress modification (both increase and decrease), induced by the screening current. In this work, we investigate such a hoop stress modification by a small coil experiment with a strain measurement and a numerical simulation. An experimental result shows a very high stress increase factor of >4.1, defined by the maximum circumferential stress over B_zJR stress, and the simulated result is in qualitative agreements. The strain (stress) shows a hysteresis effect corresponding to the screening current behavior. A large hoop stress modification causes not only a hoop stress increase, but also buckling of the conductor, which induces delamination and micro-clacks of the superconducting layer. We also show the stress modification can be reduced by bonding turns with epoxy.**

***Index Terms*—REBCO coil, inhomogeneous hoop stress, screening current, stress modification, degradation.**

I. Introduction

ONE of the most important issues to be solved for high-temperature superconducting (HTS) magnet is degradation of the performance of REBCO coils for mechanical reasons [1]. Although the REBCO conductor is strong enough to resist axial tensile stress, it is easily degraded by local stress concentrations appearing in the case of peeling/cleavage, edgewise bending and buckling [2]. Degradations are classified into the following two categories; (a) degradation due to thermal stress and (b) degradation due to electromagnetic forces [3]. The mechanism of thermal stress-induced degradation has been extensively investigated and some remedies have been proven to be effective [4]–[12]. However, in the latter case, the REBCO coil still sometimes shows degradation of the performance, although the average hoop stress, B_zJR, caused by the electro-magnetic force is far below the tolerable strength of the REBCO conductor [3], where B_z is the axial magnetic field, J is the conductor current density and R is the coil radius.

Hahn *et al.* [13] suggested that the degradation of a no-insulation (NI) REBCO double-pancake insert coil for a 45.5 T field is due to the interaction between the axial magnetic field and the screening current induced in the REBCO conductor. More recently, Ueda *et al.* [14] and Xia *et al.* [15] demonstrated stress increase by numerical simulations. However, such stress modification due to screening current has not been systematically investigated so far. Furthermore, the relation between stress modification and coil degradation has not been clarified; they are investigated in this paper. Structural features of the damaged REBCO conductor were investigated by scanning electron microscopy (SEM).

The topics investigated are (i) hoop stress modification during the external field cycle and transport current cycle using experiments and numerical simulations and (ii) hysteresis of the modified stress during sweep of the external field. Damages on a degraded REBCO coil and a remedy will be discussed.

II. Experimental

A schematic drawing of the coil experiment is shown in Fig. 1. We fabricated REBCO single-pancake dry-coils such as Coils #2 and Coil #3; three strain gauges ($\varepsilon_{\theta,\mathrm{up}}$, $\varepsilon_{\theta,\mathrm{center}}$ and $\varepsilon_{\theta,\mathrm{low}}$) were bonded to the outer surface of the outermost turn of each coil as seen in the photograph in Fig. 1. In order to measure a screening current-induced field in the radial direction, a Hall sensor was installed near the strain gauges for each coil. Parameters of the REBCO coils are listed in Table I; Coil #2 and Coil #3 have the same physical parameters. One of the test coils was fixed at the top end of the cold bore of an NbTi coil as shown in Fig. 1,

Manuscript received September 25, 2019; accepted February 12, 2020. Date of publication March 10, 2020; date of current version April 14, 2020. This work was supported in part by JST-Mirai Program under Grant JPMJMI17A2 and in part by Grant-in-Aid for JSPS Fellows under Grant 19J11812. (*Corresponding author: Yoshinori Yanagisawa.*)

Shunji Takahashi is with NMR Science and Development Division, RIKEN SPring-8 Center, Yokohama 230-0045, Japan, and also with Sophia University, Tokyo 102-8554, Japan (e-mail: shunji.takahashi@riken.jp).

Yu Suetomi is with NMR Science and Development Division, RIKEN SPring-8 Center, Yokohama 230-0045, Japan, with Chiba University Chiba 263-8522, Japan, and also with Japan Society for the Promotion of Science, Tokyo 102-0083, Japan (e-mail: yu.suetomi@riken.jp).

Tomoaki Takao is with Faculty of Science and Technology, Sophia University, Tokyo 102-8554, Japan (e-mail: t-takao@sophia.ac.jp).

Yoshinori Yanagisawa is with NMR Science and Development Division, RIKEN SPring-8 Center, Yokohama 230-0045, Japan (e-mail: yoshinori.yanagisawa@riken.jp).

Hideaki Maeda is with Japan Science and Technology Agency, Kawaguchi 332-0012, Japan, and also with NMR Science and Development Division, RIKEN SPring-8 Center, Yokohama 230-0045, Japan (e-mail: hideaki.maeda@riken.jp).

Yasuaki Takeda is with the Department of Applied Chemistry, The University of Tokyo, Tokyo 113-8656, Japan (e-mail: ytakeda@g.ecc.u-tokyo.ac.jp).

Jun-ichi Shimoyama is with the Department of Physics and Mathematics, Aoyama Gakuin University, Sagamihara 252-5258, Japan (e-mail: shimo@phys.aoyama.ac.jp).

Color versions of one or more of the figures in this article are available online at https://ieeexplore.ieee.org.

Digital Object Identifier 10.1109/TASC.2020.2974837

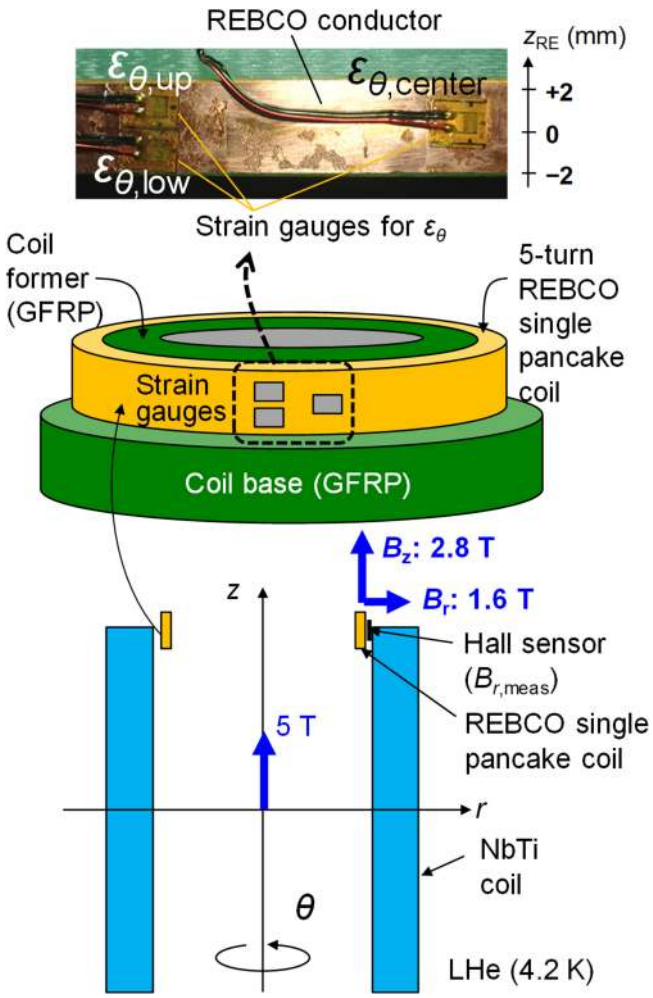

Fig. 1. Experimental apparatus for measuring hoop strain distribution of the outermost turn of a REBCO single pancake coil under external magnetic fields in liquid helium.

TABLE I
PARAMETERS OF REBCO SINGLE PANCAKE COILS AND A NBTI COIL

	REBCO coil (#2 and #3)	NbTi coil
Conductor	SuperPower, SCS4050	NbTi
Conductor width / thickness (mm)	4.0 / 0.1	-
Conductor critical current at 77 K (A)	114	-
Winding	Single pancake (Superconducting layer inside)	Layer-wound
Inter-turn insulation	Polyimide tape	-
Coil I.D. / O.D. / height (mm)	79.5 / 81.3 / 4.2	95.0 / 105 / 160
Number of turns	5	-
Operating current (A)	300	156
Center field (T)	0.024	5
External field at the winding at an NbTi coil current of 156 A (T)	B_z: 2.8 B_r: 1.6	-
Estimated critical current at 4.2 K in the external field (A)	912	-
B_zJR^* (MPa)	84	-

*J: conductor current density, R = O.D./2

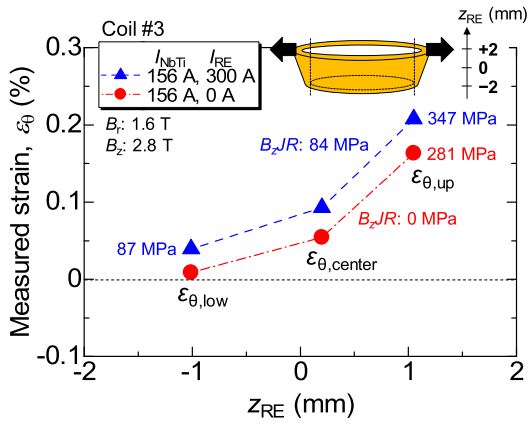

Fig. 2. Measured strain distributions in a REBCO single pancake coil with and without a transport current under an external magnetic field. The vertical axis does not include strain produced by the effect of bending and cooling. The stresses are obtained from the stress-strain characteristics obtained by the numerical model described in section IV.

which was tested in liquid helium at 4.2 K. We measured the strains for the outermost turn of the test coil under the external magnetic field $B_z = 2.8$ T and $B_r = 1.6$ T generated by the outer NbTi coil, with and without a transport current in the REBCO coil.

III. EXPERIMENTAL RESULTS

A. Inhomogeneous Hoop Strain (Stress)

The closed triangles in Fig. 2 show conductor strains measured for Coil #3 just after holding the external magnetic field generated by the NbTi coil; the horizontal axis gives the position in the width direction. Even in the case of zero current, a circumferential strain as high as 0.16% appears at the upper part of the conductor, while it is nearly zero at the lower part of the conductor; the 0.16% strain corresponds to 281 MPa based on the stress-strain characteristics obtained from the numerical model described in the next section. They are caused by the electromagnetic force resulting from the interaction between the axial-magnetic field and the screening current; their directions are outward at the upper part whereas inward at the lower part.

The strains, $\varepsilon_{\theta,\mathrm{up}}$, $\varepsilon_{\theta,\mathrm{center}}$ and $\varepsilon_{\theta,\mathrm{low}}$, increase with the coil transport current, as the electromagnetic force is modified; e.g., for 300 A, they are 0.21%, 0.09% and 0.04%, respectively. The 0.21% and 0.04% strains correspond to stresses of 347 MPa and 87 MPa, respectively. Considering the strain distribution in Fig. 2, the maximum hoop stress, $\sigma_{\theta,\max}$, and the minimum hoop stress, $\sigma_{\theta,\min}$, should be >347 MPa and <87 MPa, respectively. Therefore the stress increase factor, defined as $\sigma_{\theta,\max}/B_zJR$, is >4.1 (= 347/84), while the stress decrease factor, defined as $\sigma_{\theta\min}/B_zJR$, is <1.04 (= 87/84). After holding the external magnetic field, $\varepsilon_{\theta,\mathrm{up}}$ showed a negative drift with time, which was caused by relaxation of the screening currents.

Thus, this data clearly demonstrates that the inhomogeneous hoop strain distribution in the width direction seen in Fig. 2 is mainly dominated by the effect of the screening current induced by the cycling of the external magnetic field.

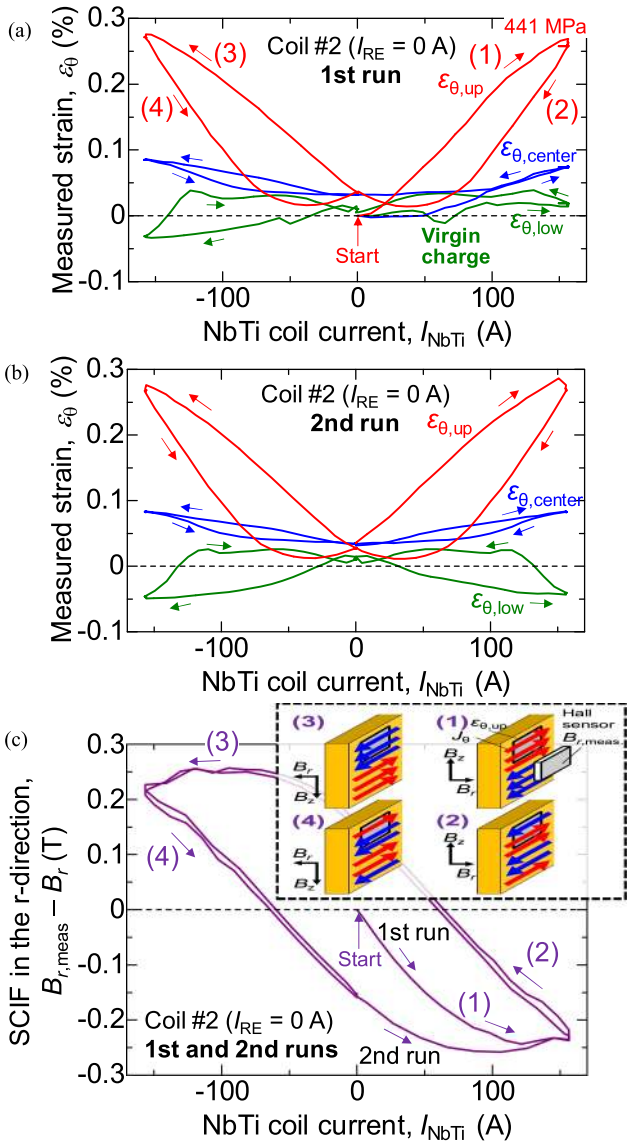

Fig. 3. (a) Measured hysteresis effect of strains ($\varepsilon_{\theta,\mathrm{up}}$, $\varepsilon_{\theta,\mathrm{center}}$, and $\varepsilon_{\theta,\mathrm{low}}$) under a NbTi coil field sweep without transport current of the REBCO single pancake coil. The stress of 441 MPa is obtained from the stress-strain characteristics obtained by the numerical model described in section IV. (b) Measured hysteresis effect of strains ($\varepsilon_{\theta,\mathrm{up}}$, $\varepsilon_{\theta,\mathrm{center}}$, and $\varepsilon_{\theta,\mathrm{low}}$): 2nd run obtained after the 1st run shown in (a). (c) Screening current-induced field (SCIF) in the radial direction obtained by substituting the external radial magnetic field of the NbTi coil, B_r, from the measured radial magnetic field, $B_{r,\mathrm{meas}}$. Inset: Schematic drawings of the current distribution in the REBCO conductor. Numbers (1), (2), (3), and (4) correspond to the charging processes indicated by the arrows (1), (2), (3), and (4) in Figs. (a) and (b).

B. Hysteresis Effect of Hoop Strain (Stress)

Figs. 3(a) and 3(b) show a hysteresis behavior of $\varepsilon_{\theta,\mathrm{up}}$, $\varepsilon_{\theta,\mathrm{center}}$ and $\varepsilon_{\theta,\mathrm{low}}$ for Coil #2, during a positive/negative charge/discharge of an NbTi coil; the REBCO coil current was kept at 0 A (i.e., $I_{\mathrm{RE}} = 0$ A); note that the horizontal axis corresponds to the external field strength. Fig. 3(a) is the 1st test run, while Fig. 3(b) is the subsequent 2nd test run. Such a hysteresis behavior of the strain has not been reported before.

Fig. 3(c) plots a hysteresis loop of the radial component of screening current-induced field (SCIF) near the strain gauges, measured with the Hall sensor indicated in Fig. 1 (see the bottom figure). As demonstrated previously [1], the SCIF shows a significant hysteresis effect during the current cycle of the external field; this is usually explained using arguments based on the Bean model.

As seen in Fig. 3(a), $\varepsilon_{\theta,\mathrm{up}}$ increases in the positive direction (i.e., tensile strain) with the external field during the first positive charge, indicated by the arrow (1) in Fig. 3(a); the curve is smaller during the discharge of the external coil, indicated by the arrow (2) in Fig. 3(a). Similar hysteresis is observed in the negative charge/discharge process (see the arrows (3) and (4) in Fig. 3(a), respectively). Hysteresis for $\varepsilon_{\theta,\mathrm{center}}$ is similar, although 3 to 4-fold smaller than $\varepsilon_{\theta,\mathrm{up}}$. To the contrary, hysteresis behavior for $\varepsilon_{\theta,\mathrm{low}}$ is different. During the first charge, $\varepsilon_{\theta,\mathrm{low}}$ increases with the external field in the negative direction (i.e., compressive strain), while it becomes positive during the discharge process. The behavior is seen more clearly in the negative charge/discharge process on the left.

The hysteresis effect during the positively charged process is interpreted as follows; as the external field is increased, positive and negative screening current gradually penetrates from the upper and lower ends of the conductor respectively, as seen in the inset of Fig. 3(c). Both this effect and increase in the axial magnetic field results in the gradual increase shown by the arrow (1) in Fig. 3(a). During the discharge process, negative current penetrates from the top end with positive current from the bottom end, which are superimposed on the remnant current described above; see the inset (2) in Fig. 3(c) [16]. This results in a smaller strain than that in the charge process; see the arrow (2) in Fig. 3(a). The hysteresis for the negative charge and discharge are bilaterally symmetrical.

The hysteresis loop in the 1st run seen in Fig. 3(a) is slightly different from other loops. Here, $\varepsilon_{\theta,\mathrm{up}}$ increases from 0% to 0.27% in the first charge process, while it decreases to 0.03% in the discharge process; the remnant strain is due to the plastic deformation of the conductor. Similar behavior is also observed for $\varepsilon_{\theta,\mathrm{center}}$. To the contrary, $\varepsilon_{\theta,\mathrm{low}}$ is dissimilar; the positive tensile strain superimposes on the negative compressive strain above 70 A, as seen in Fig. 3(a). It is suggested that the superimposed tensile strain may be due to deformation by buckling of the winding; as the coil winding can be modeled as a thin cylinder under external pressure, it is reasonable to assume the appearance of buckling. This point will be discussed later with regard to the performance degradation of Coil #3 after the test runs.

IV. Numerical Simulation

A. Numerical Simulation Model

We carried out a numerical simulation of inhomogeneous hoop stress in the 5-turn REBCO single pancake coil in the external field of the NbTi coil.

A screening current distribution in the REBCO conductor in the coil was calculated using the superconductor thin strip model under self and external fields [17]–[19], which simulated transient behavior of screening currents. The width and thickness of the superconducting layer were 4.0 mm and 1 μm, respectively. Critical current and n-index were 912 A and 24, respectively. In order to simulate the experiment, the external radial magnetic field and the REBCO coil current were swept from 0 T to 1.6 T

TABLE II
MECHANICAL PROPERTIES OF REBCO CONDUCTOR MATERIALS

	Young's modulus (GPa)	Poisson's ratio
REBCO layer [21]	157	0.3
Copper stabilizer [21]	98	0.34
Hastelloy substrate [21]	228	0.307
Polyimide insulator [22]	3.4	0.34

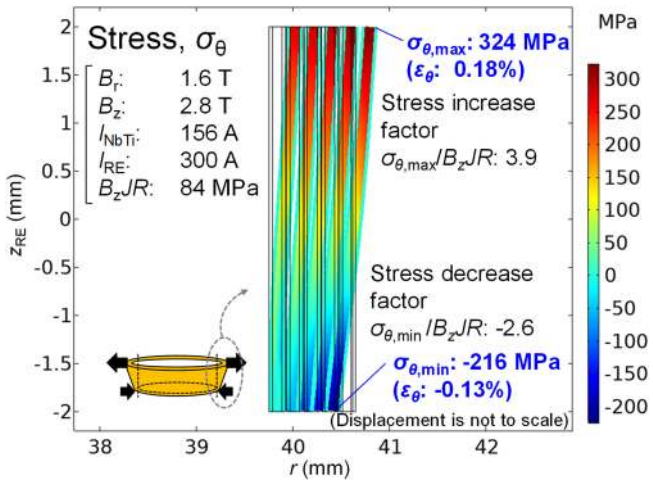

Fig. 4. Simulated stress distribution in the REBCO single pancake coil with a transport current under an external magnetic field.

and from 0 A to 300 A in 1,170 seconds. The Lorentz force distribution in the superconducting layer was obtained from production of the screening current density distribution and the magnetic field distribution. For simplicity, magnetic coupling between each turn was neglected.

Then, we made an axisymmetric structural analysis model of the 5-turn REBCO coil for obtaining a hoop stress distribution using the Solid Mechanics interface of the commercial FEM software COMSOL Multiphysics [20]. The REBCO conductor was composed of a REBCO layer, a copper stabilizer and a Hastelloy substrate, whose thick-nesses were 1, 40 and 50 μm, respectively, which was modeled as a 0.1 mm-thick orthotropic elastic material as reported in ref. [21]. The silver layer and buffer layer were neglected since they are both very thin. The use of 35 μm-thick polyimide insulators for both sides of each turn were also considered. The mechanical properties of each material component are listed in Table II. In addition, gap elements between each turn were considered to model a dry winding coil. For the boundary condition, contact pairs are defined between adjacent turns. Furthermore, the radial displacement at the coil inner periphery and the axial displacement at the coil lower end were not allowed to be negative considering the existence of the coil former and the coil base seen in Fig. 1. The entire element in the model was meshed into 36,000 square elements. By using this model under the Lorentz forces generated by the screening current as the body forces to the conductor, the stress distribution was analyzed.

B. Strain Distribution

Fig. 4 shows a simulated stress distribution in the cross-section of the REBCO coil with a transport current of 300 A just after

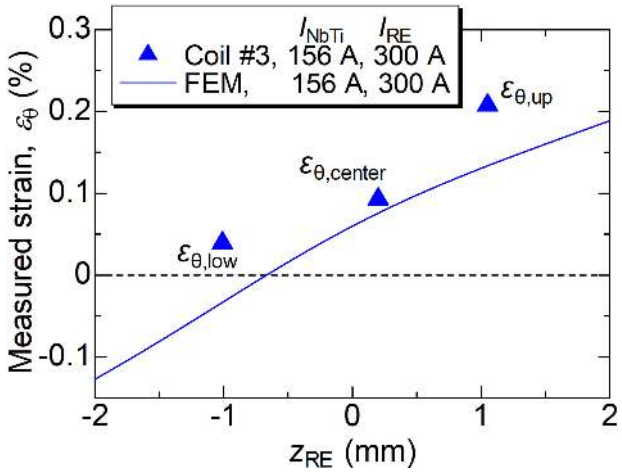

Fig. 5. Comparison between simulated and measured strain distributions in the REBCO single pancake coil with a transport current under an external magnetic field.

holding the external field of the NbTi coil. The cross-section shows a coil deformation with enlargement of the upper part (324 MPa; 0.18%) and shrinking of the lower part along the radial direction (−216 MPa; −0.13%), which gives a stress increase factor of 3.9 (= 324/84) and a stress decrease factor of −2.6 (= −216/84). Note that these stress/strain values are those of the outer surface of the REBCO conductor modeled as a 0.1 mm-thick homogenized orthotropic elastic material [21].

Fig. 5 compares the simulated hoop strain distribution along the conductor width direction to the measured strains shown in Fig. 2. The simulated result qualitatively agrees with the measured strain distribution although the polarities of the lower part, i.e., $\varepsilon_{\theta,\mathrm{low}}$-part, are different. In the experiment, friction between the bottom of the coil and the coil base beneath the coil might interfere with the radial displacement of the conductors towards the inner direction. Further discussions are presented in the next section.

V. DISCUSSION

A. Degradation in Coil Performance

If a local hoop stress at the top end of a REBCO conductor is excessively enhanced by the effect of screening current, the coil performance may be degraded. In our previous paper [2], inhomogeneous tensile strain has been reported, where both hoop stress and edgewise bending were applied simultaneously to a REBCO conductor. It gives rise to micro-cracks in a half of the conductor, which degrades the conductor critical current. Thus, it is probable that stress modification seen in Figs. 4 and 5 due to screening current results in critical current degradation due to micro-cracks.

In order to clarify this issue, we made a postmortem examination of Coil #3 after conducting the coil tests described in Fig. 2. The coil critical current, $I_{\mathrm{c,coil}}$, at 77 K was degraded from 70 A to 30 A. The lower end of the outermost turn was deformed in a wavy fashion resembling buckling as seen in Fig. 6 (schematic) and Fig. 7(a) (photo); three convex parts are indicated by the $\times$-marks in Fig. 6, one of which is seen in

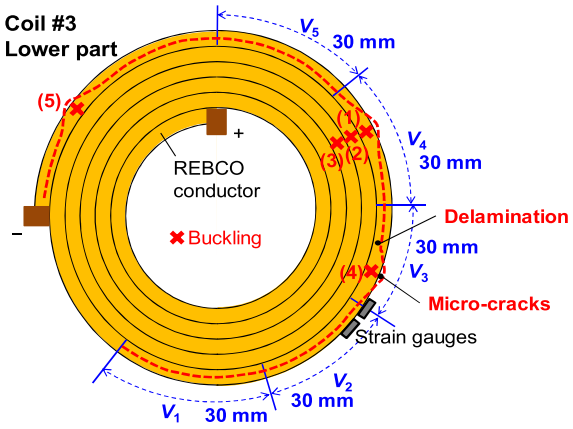

Fig. 6. Schematic of damaged part for the lower half part of Coil #3.

Fig. 7(a). As a lower half of the conductor is considered to be a thin-walled cylinder under external pressure, buckling is thus easily induced. Buckling is also proved by the appearance of the hysteresis loop for the 1st charge seen in Fig. 3(a) as described previously. As shown by the open square in Fig. 8, the critical current for the lower half of the conductor near the wavy part was enormously degraded, while the upper half was not; note that the conductor piece corresponds to V_3 seen in Fig. 6. After this experiment, we chemically removed the copper stabilizer and silver protection layer from this REBCO conductor; the surface of the lower half was observed with an optical microscope and a SEM. Notable delamination of the REBCO layer was found near the lower periphery of the conductor as shown in Fig. 7(b) observed with an optical microscope and Fig. 7(c) with SEM; the delamination is at a foot of a convex as indicated in Fig. 6. In addition, micro-cracks were found at a convex part (see Fig. 6) as seen in Fig. 7(d); the length of a micro-crack was $\sim$200 μm along the conductor width direction. Thus, it is demonstrated that buckling of the lower half of the conductor induces delamination and micro-cracks, resulting in degradation of the coil critical current.

The appearance of buckling may be affected by mechanical mobility of the conductor including friction on the coil base and the existence of soft polymer insulation between coil turns. It is suggested that the upper periphery of the conductor was enlarged by a positive hoop stress enhanced by the screening current, while the lower periphery was deformed with buckling under a negative hoop stress as described in Fig. 9. In the present experiment on Coil #3, the enhanced hoop stress at the upper periphery does not exceed the irreversible stress limit of the conductor [23], while the buckling at the lower periphery produce delamination and micro-cracks, causing degradation in the conductor performance. The upper and lower peripheries of the superconducting layer had many pre-existing cracks produced by the slitting process which were made during conductor manufacturing [11], [13] and it is probable that such pre-existent cracks are the origination of the delamination under buckling. The inset in Fig. 7(b) implies that the delamination propagated along the pre-existing cracks.

The coil deformation shown in Figs. 6 and 9 can explain the discrepancy between the measured strain and the simulated strain for the conductor lower part shown in Fig. 5 as there should

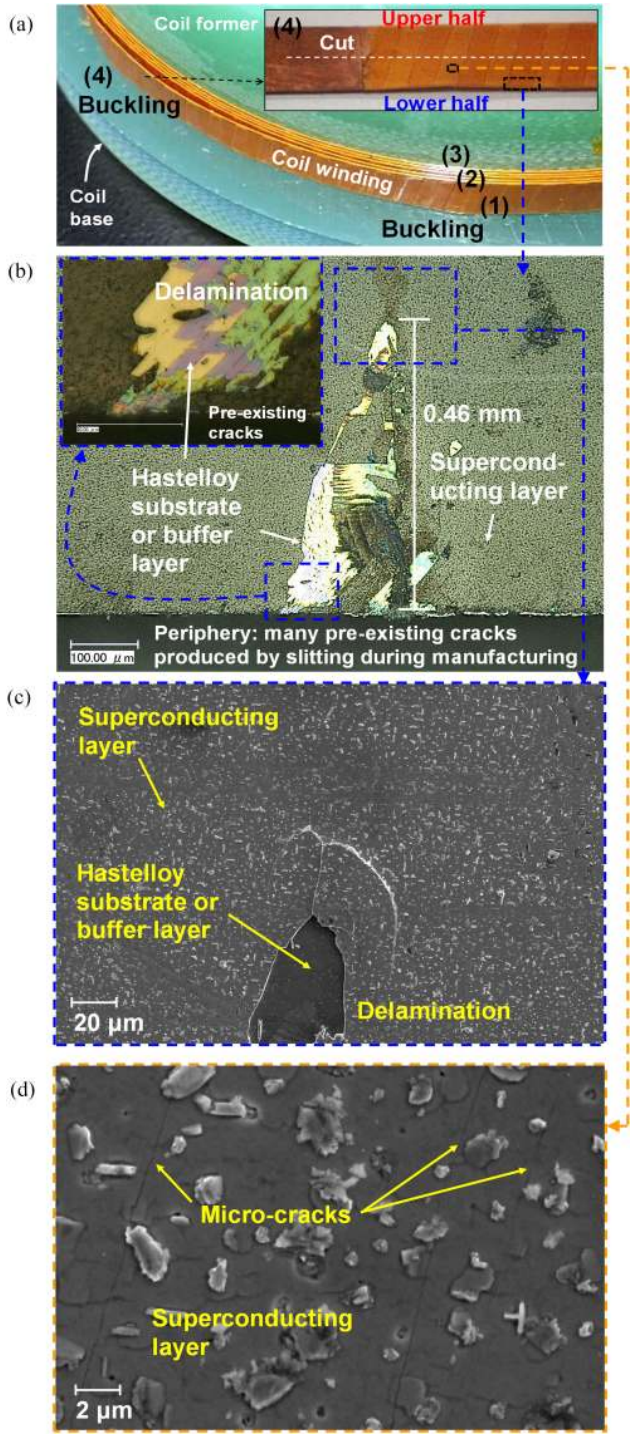

Fig. 7. (a) Conductor deformation of Coil #3 after the experiment at 4.2 K in the external field. (b) Partial delamination of the superconducting layer of a degraded part. (c) SEM image of the delamination part. (d) SEM image of a part with micro-cracks.

be strain distribution along the coil circumferential direction in the actual coil, while the two-dimensional simulation could not consider the buckling effect.

For a more comprehensive understanding of the conductor degradation, more observations with a SEM are necessary, which are being made in our laboratory.

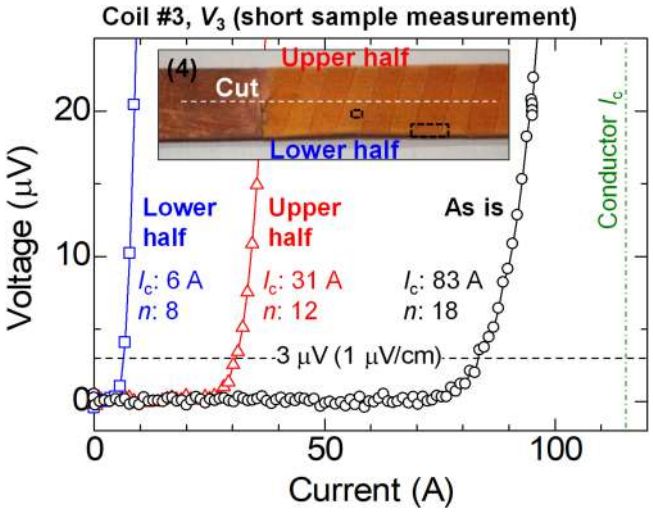

Fig. 8. Voltage-current characteristics of a degraded part (V_3) of Coil #3 shown in Fig. 7(a).

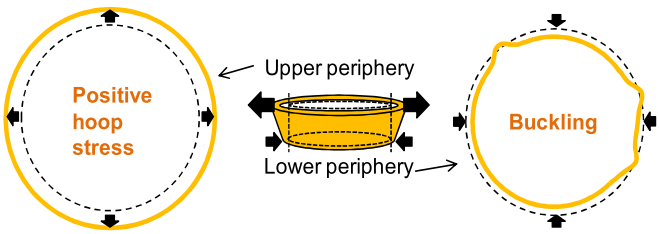

Fig. 9. Schematic of deformation of a REBCO single pancake coil under the hoop stress modification due to the screening current.

B. *Effect of Epoxy Bonding on Suppression of Stress Modification*

As a remedy for the hoop stress modification due to screening currents, the effect of epoxy bonding of the coil was numerically discussed. Fig. 10(a) shows the bonded-turn number dependence of the stress increase factor ($\sigma_{\theta,\max}/B_zJR$: open circles) and the stress decrease factor ($\sigma_{\theta,\min}/B_zJR$: open triangles) on the 5-turn REBCO coil model as shown in Fig. 10(a'). The horizontal axis is the number of bonded-turns, $N_{\rm bond}$, from the outermost layer. The Lorentz force distribution is the same as described above. The stress increase factor is reduced to 3.06 for a fully bonded winding ($N_{\rm bond} = 5$) from 3.84 for a dry-winding, while the hoop stress decrease factor is raised to -0.50 from -2.53. This result indicates epoxy bonding between turns suppresses the stress modification, owing to an increase in the mechanical rigidity of the coil winding.

In order to observe the effects of $N_{\rm bond}$ on the stress modification, we also made a simulation with a many-turn coil model as shown in Fig. 10(b'). In this model, all turns are bonded and the same Lorentz force distribution was assumed for each turn for simplicity. Fig. 10(b) shows that both the stress increase and decrease factors gradually approaches 1.0 with increasing $N_{\rm bond}$, respectively reaching 1.0 and 0.49 at $N_{\rm bond} = 50$, i.e., stress modification (both increase and decrease) is suppressed. Thus sufficient epoxy bonding may prevent both over hoop stress and buckling seen in Fig. 9. However, an epoxy impregnated

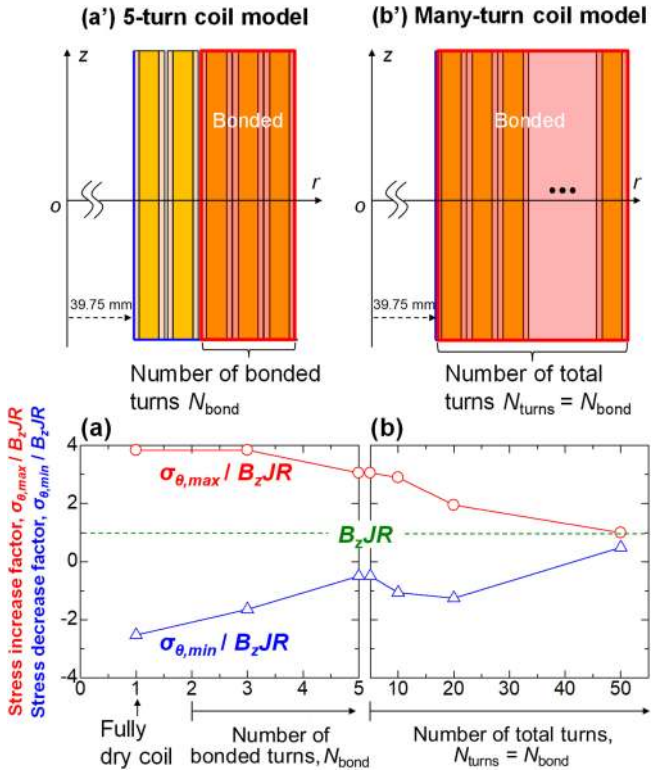

Fig. 10. (a) Bonded-turn number dependence of the stress increase and decrease factors on the 5-turn REBCO coil model as shown in (a'). (b) Total turn number dependence of the stress increase and decrease factors on the many-turn coil model in which all the turns are bonded as shown in (b').

coil sometimes degrades due to a thermal stress during cooling [4]. Therefore a thermal stress must be suppressed by such as methods as those reported in refs. [5]–[12].

VI. Conclusion

We measured hoop strain distributions in a REBCO single pancake coil at 4.2 K under an external magnetic field. Our conclusions are as follows.

1) We experimentally demonstrated an inhomogeneous hoop stress in a REBCO single pancake coil caused by the screening current, which produces a substantial increase of the local hoop stress.
2) The stress inhomogeneity is dominated by the screening current and therefore shows hysteresis.
3) An inhomogeneous hoop stress makes compressive strain for a conductor periphery. It can result in buckling, causing delamination and micro-cracks, and resultant degradation.
4) Epoxy bonding between turns increases the mechanical rigidity of the winding, resulting in a decrease in the stress modification (both increase and decrease). This may be a remedy against this problem although thermal stress-induced degradation still needs to be taken into account.

Acknowledgment

The authors would like to thank Y. Matsutake of Sophia University / RIKEN for providing useful comments for the coil experiment.

REFERENCES

[1] H. Maeda and Y. Yanagisawa, "Recent developments in high-temperature superconducting magnet technology (review)," *IEEE Trans. Appl. Supercond.*, vol. 24, no. 3, Jun. 2014, Art. no. 4602412.

[2] K. Kajita *et al.*, "Degradation of a REBCO conductor due to an axial tensile stress under edgewise bending: A major stress mode of deterioration in a high field REBCO coil's performance," *Supercond. Sci. Technol.*, vol. 30, no. 7, 2017, Art. no. 074002.

[3] T. Matsuda *et al.*, "Degradation of the performance of and epoxy-impregnated REBCO solenoid due to electromagnetic forces," *Cryogenics*, vol. 90, pp. 47–51, 2019.

[4] T. Takematsu *et al.*, "Degradation of the performance of a YBCO-coated conductor double pancake coil due to epoxy impregnation," *Phys. C, Supercond.*, vol. 470, no. 17–18, pp. 674–677, 2010.

[5] U. P. Trociewitz *et al.*, "35.4 T field generated using a layer-wound superconducting coil made of (RE)$Ba_2Cu_3O_{7-x}$ (RE = rare earth) coated conductor," *Appl. Phys. Lett.* vol. 99, 2011, Art. no. 202506.

[6] C. Barth *et al.*, "Degradation free epoxy impregnation of REBCO coils and cables," *Supercond. Sci. Technol.*, vol. 26, 2013, Art. no. 055007.

[7] H. Song, P. Brownsey, Y. Zhang, J. Waterman, T. Fukushima, and D. Hazelton, "2G HTS coil technology development at SuperPower," *IEEE Trans. Appl. Supercond.*, vol. 23, no. 3, Jun. 2013, Art. no. 4600806.

[8] X. Jin *et al.*, "Study on the mechanism of preventing degradation in the performance of REBCO coils," *IEEE Trans. Appl. Supercond.*, vol. 24, no. 3, Jun. 2014, Art. no. 4600104.

[9] I. Kesgin *et al.*, "Degradation free vacuum epoxy impregnated short REBCO undulator magnets," *IOP Conf. Ser.: Mater. Sci. Eng.*, vol. 279, 2017, Art. no. 012009.

[10] H. Miyazaki, S. Iwai, T. Tosaka, K. Tasaki, and Y. Ishii, "Degradation-free impregnated YBCO pancake coils by decreasing radial stress in the windings and method for evaluating delamination strength of YBCO-coated conductors," *IEEE Trans. Appl. Supercond.*, vol. 24, no. 3, Jun. 2014, Art. no. 4600905.

[11] Y. Yanagisawa *et al.*, "Remarkable weakness against cleavage stress for YBCO-coated conductors and its effect on the YBCO coil performance," *Phys. C, Supercond.*, vol. 471, no. 15–16, pp. 480–485, 2011.

[12] Y. Yanagisawa *et al.*, "Removal of degradation of the performance of an epoxy impregnated YBCO-coated conductor double pancake coil by using a polyimide-electrodeposited YBCO-coated conductor," *Phys. C, Supercond.*, vol. 476, pp. 19–22, Jun. 2012.

[13] S. Hahn *et al.*, "45.5-tesla direct-current magnetic field generated with a high-temperature superconducting magnet," *Nature*, vol. 570, pp. 496–499, 2019.

[14] H. Ueda *et al.*, "Numerical simulation on electromagnetic force and stress in HTS tape in coil winding," presented at Annual Conf. Cryogenics Supercond. Soc. Japan, Yamagata, Japan, 2018, pp. 19–21.

[15] J. Xia *et al.*, "Stress and strain analysis of a REBCO high field coil based on the distribution of shielding current," *Supercond. Sci. Technol.*, vol. 32, 2019, Art. no. 095005.

[16] Y. Yanagisawa *et al.*, "Effect of current sweep reversal on the magnetic field stability for a Bi-2223 superconducting solenoid," *Phys. C, Supercond.*, vol. 469, no. 22, pp. 1996–1999, 2009.

[17] E. H. Brandt, "Thin superconductor in a perpendicular magnetic AC field: General formulation and strip geometry," *Phys. Rev. B*, vol. 49, pp. 9024–9040, 1994.

[18] T. Yazawa *et al.*, "Numerical calculation of current density distribution in high temperature superconducting tapes with finite thickness in self field and exernal field," *Phys. C*, vol. 310, pp. 36–41, 1998.

[19] Y. Yanagisawa *et al.*, "Effect of YBCO-coil shape on the screening current-induced magnetic field intensity," *IEEE Trans. Appl. Supercond.*, vol. 20, no. 3, pp. 744–747, Jun. 2010.

[20] "COMSOL Multiphysics," COMSOL Inc. Burlington, MA, USA. [Online]. Available: http://www.comsol.com/comsol-multiphysics

[21] Y. Yang, H. Yong, and Y. Zhou, "Electro-mechanical behavior in arrays of superconducting tapes," *J. Appl. Phys.*, vol. 124, no. 7, 2018, Art. no. 073902.

[22] J. W. Ekin, *Experimental Techniques for Low-Temperature Measurements*. New York, NY, USA: Oxford, 2006

[23] C. Barth *et al.*, "Electro-mechanical properties of REBCO coated conductors from various industrial manufacturers at 77 K, self-field, and 4.2 K, 19 T," *Supercond. Sci. Technol.*, vol. 28, 2015, Art. no. 045011.